Analysis of direct tunneling current from quasi-bound states in n-MOSFET based on non-equilibrium Green's function

Satoru Muraoka, Satofumi Souma, and Matsuto Ogawa
Department of Electrical and Electronics Engineering, Kobe University
1 Rokkodai, Nada, Kobe, 657-8501, JAPAN
Email: 070t222t@stu.kobe-u.ac.jp

***Abstract*—Gate-leakage current from quasi-bound states in highly scaled metal-oxide-semiconductor devices has been investigated by using a non-equilibrium Green's function method. We have taken account of the realistic band structure of Si with anisotropic effective masses. This study also presents a model for the efficient simulation of gate-leakage current with open boundaries where no escape time or life time has been assumed contrary to the conventional analysis [1]. We have added optical potential to the on-site energies only above the conduction band edge in the substrate electrode. The optical potential induces energy broadening in the triangle potential to calculate the density of states properly.**

I. Introduction

Aggressive scaling down of metal-oxide-semiconductor field-effect transistors (MOSFETs) continues to push the gate lengths into the deca-nanometer regime. According to ITRS [2], for sub-100 nm gate-length devices, the gate-oxide thickness has become as thin as 2 nm or less. At such gate-oxide thicknesses, a substantial current flows through the oxide due to direct tunneling of carriers from substrate to gate electrode, which remains one of the major limitations to further minitualization. This current not only adversely affects the MOS devices performance but also greatly increases the standby power consumption of highly integrated circuits. Therefore, it is quite important to understand the tunneling phenomena and calculate the direct tunneling current in such ultimately scaled-down MOSFETs. The aim of this paper is to understand the effect of the oxide thickness and gate voltage on direct tunneling current from the quasi-bound states (QBSs) formed in the inversion layer with the open boundary conditions.

II. Simulation Method and Device Model

The direct tunneling current from QBSs calculations are carried out using the one-dimensional non-equilibrium Green's function (NEGF) formalism based on the effective-mass theory, which properly takes into account quantum effect in the devices. In this work, electron density calculated by NEGF and electrostatic potential calculated by Poisson's equation are solved self-consistently to obtain both potential profile and carrier density distribution, and the tunneling current is calculated after the self-consistency is satisfied. Then the current density may be calculated by the Tsu-Esaki's formula

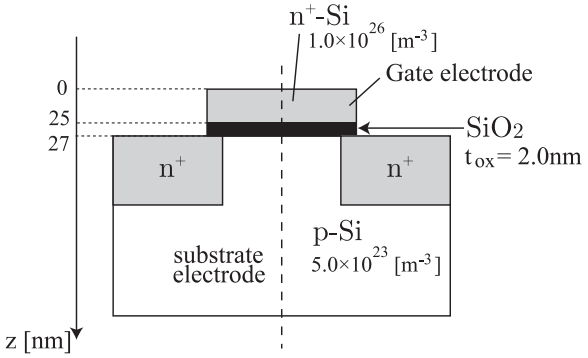

Fig. 1. Schematic n-MOS model in the present work. The tunneling current is assumed to flow along the broken line in z direction.

expressed in terms of the NEGF or Fisher-Lee relationship [3].

Our device structure is described using the retarded Green's function obtained from the following equation for each electron energy

$$G = [E_z I - H_L - \Sigma_1 - \Sigma_2]^{-1}, \tag{1}$$

$$H_L = E_c - \frac{\hbar^2}{2m_z^*}\frac{d^2}{dz^2} + U_c(z), \tag{2}$$

where H_L is longitudinal part of Hamiltonian, and $\Sigma_{1,2}$ are appropriate boundary self-energies which replace the effect of the gate and substrate electrodes. These are matrices with the same dimension as the device Hamiltonian, even though the contacts themselves are much larger entities. In Eq. (2), E_c is the conduction band bottom, m_z^* is effective mass in the direction perpendicular to the interface, and $U_c(z)$ is the electrostatic potential. Carrier concentration is then given by

$$n(z) = \int \frac{dE_z}{2\pi}[F_1(E_z-\mu_1)A_1 + F_2(E_z-\mu_2)A_2], \tag{3}$$

$$\begin{aligned} F_{1,2}(E_z-\mu_{1,2}) &= \sum_{k_{||}} f_{1,2}(E_z + E_{||} - \mu_{1,2}) \\ &= \frac{m_{||}^* k_B T}{\pi\hbar^2}\ln[1+\exp(\frac{\mu_{1,2}-E_z}{k_B T})], \end{aligned} \tag{4}$$

where $f_{1,2}$ are Fermi-Dirac distribution functions and $\mu_{1,2}$ are the Fermi energies. The subscripts 1, 2 represent the gate

978-1-4244-1753-7/08/$25.00 ©2008 IEEE

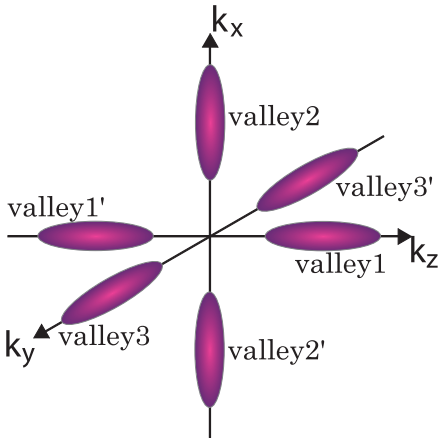

Fig. 2. 6 rotated ellipsoides in Si band structure

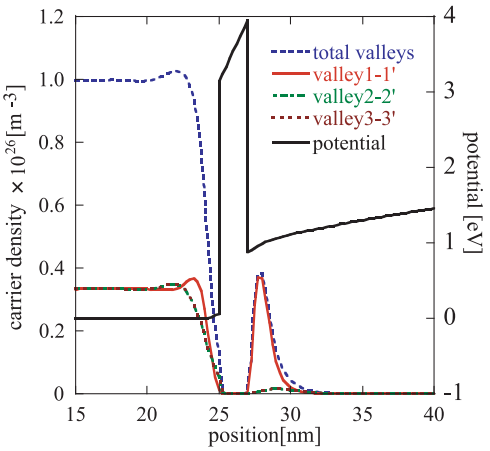

Fig. 3. The conduction band edge of the n-MOS device and electron concentration in each valley at gate bias of 1.0V

electrode and substrate electrode, respectively. In Eq. (3), the spectral functions, A, is calculated as

$$[A(E_z)] \equiv i\left([G(E_z)] - [G(E_z)]^\dagger\right), \quad (5)$$

then local density of states (LDOS) is represented as $\frac{[A(E_z)]}{2\pi}$.

The transmitted current density is given by Esaki-Tsu formula

$$J = \frac{2em^* k_B T}{(2\pi)^2\hbar^3}\int_0^\infty dE_z T(E_z)\ln\left[\frac{1+\exp(\frac{\mu_2 - E_z}{k_B T})}{1+\exp(\frac{\mu_1 - E_z}{k_B T})}\right], \quad (6)$$

where $T(E)$ is the transmission coefficient which can be expressed in terms of the Green's function as

$$T(E_z) = \mathrm{Tr}[\Gamma_2 G \Gamma_1 G^\dagger] \quad (7)$$

where $\Gamma_{1,2}$ are broadening functions represented by imaginary part of the self energy as

$$\Gamma_{1,2} = i\left([\Sigma_{1,2}] - [\Sigma_{1,2}]^\dagger\right). \quad (8)$$

In the present study, we have added optical potential (OP), $-i\eta$, to the on-site energies only above the conduction band edge in the substrate electrode. The OP induces energy broadening in the triangle potential to calculate the density of states properly. The value of η is set to zero for energies below the conduction band edge to avoid unrealistic band tail, and the value of η above the conduction band edge is 5.0 meV. Therefore, in the device, where current is calculated, current is conserved. We note that, without OP it is difficult to calculate the density of states, because broadening in energy spectrum of QBS is too narrow. In this case the OP has nothing to do with scattering.

III. Results and Discussion

Results of numerical calculations for n-MOS devices are presented in this section. The doping concentration is assumed to be $N_\mathrm{D} = 6.0\times10^{26}$ m^{-3} in the gate electrode, and $N_\mathrm{A} = 5.0\times10^{23}$ m^{-3} in the substrate, respectively. The device structure under investigation is schematically shown in Fig. 1.

The oxide thickness t_ox is 2.0 nm. The region of gate electrode is 0 - 25 nm, of oxide is 25 - 27 nm and of substrate electrode is 27 nm -. We assume that the band structure of Si is comprised of equivalent 6 ellipsoides as shown in Fig. 2, where

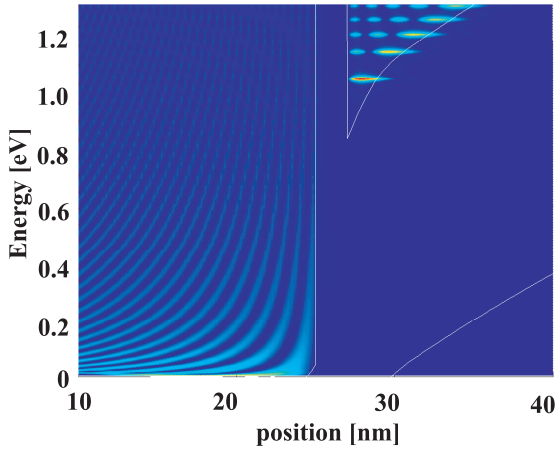

(a) valley1-1′

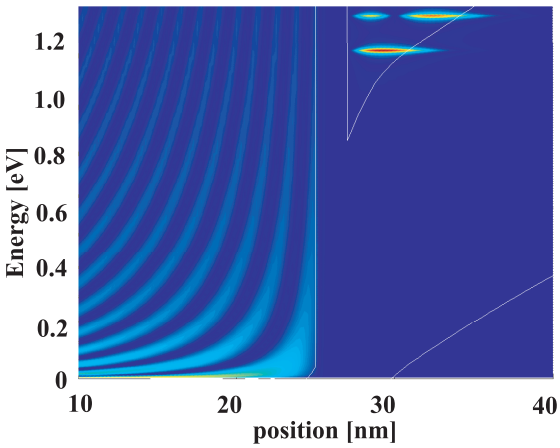

(b) valley2-2′,3-3′

Fig. 4. Local density of states, band profile, and quasi-bound-states in the MOS structure at the same bias as Fig. 3.

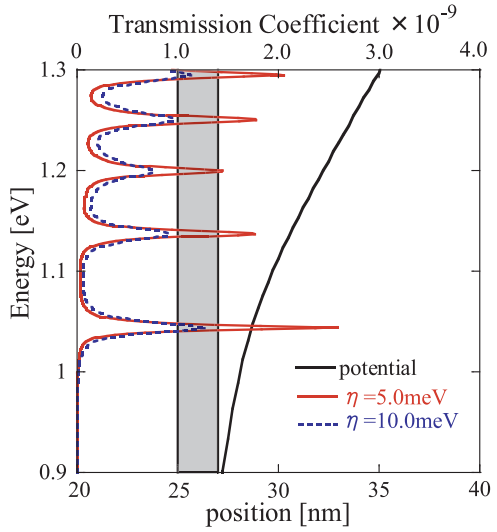

(a) valley 1-1′

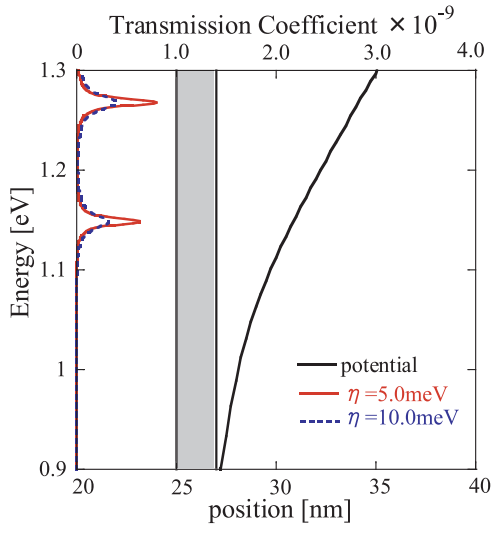

(b) valley2-2′, 3-3′

Fig. 5. Transmission coefficients from the QBSs as a function of enegy and the magnitude of OP at a bias gate bias of 1.0 V. The conduction band profile is also drawn.

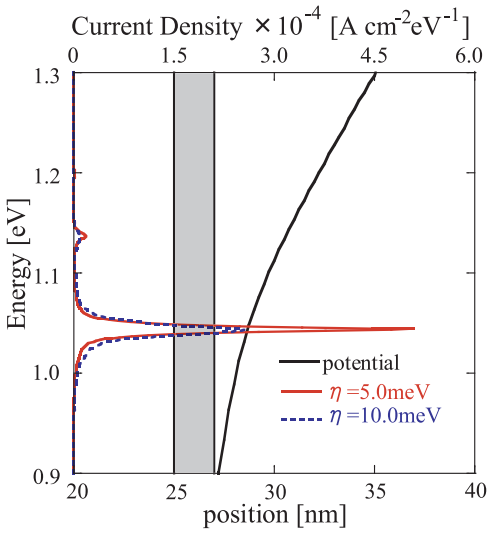

(a) valley 1-1′

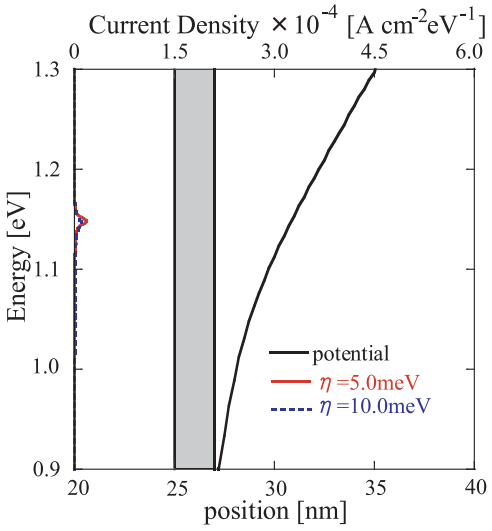

(b) valley 2-2′, 3-3′

Fig. 6. Energy spectra of the current density as a function of the magnitude of the OP.

electron effective masses are $m_l = 0.91m_0$ for the two-fold degenerate valleys, $m_t = 0.19m_0$ for the four-fold degenerate valleys in the Si substrate, and $m_{\rm ox} = 0.61{\rm m}_0$ has been chosen for the electron effective masses in the oxide. Self-consistent numerical results of potential profile and electron density distribution that take into account of the realistic band structure of Si with anisotropic effective masses are shown in Fig. 3. In the triangle potential, the carrier density of total valleys is mostly comprised of carriers in the valley 1-1′, which have the heavy effective mass m_l in the confinement direction. The peak of the electron concentration in the substrate is due to the inversion electrons. The depletion layer is also observed between the gate-electrode and the oxide. More importantly, a hump of the electron concentration in the gate region is seen, which is due to the reflection of electron waves from the oxide barrier. This hump due to electron reflection was not observed in the conventional calculation [1].

Figure 4 (a) shows LDOS in the valley 1-1′, and Fig. 4 (b) shows that in valley 2-2′, 3-3′. While the white solid lines show both the conduction and valence band edges, the brighter regions in the figure represent high DOS. In the triangle potential well, several QBSs are seen. The LDOS of each QBS in the triangle well shows obvious broadening in energy due to OP.

Fig. 5 and 6 show transmission coefficient and current density distribution flowing through the oxide in valley 1-1′ and valley 2-2′, 3-3′, respectively. Results for various values of OP are compared. Although the broadenings seen in both the transmission coefficient and the current density spectrum are proportional to the value of OP, it is verified that the position of each peak and the total current (current density integrated as a function of electron energy) are independent of the value of OP. In Fig. 5, we find that the peaks of

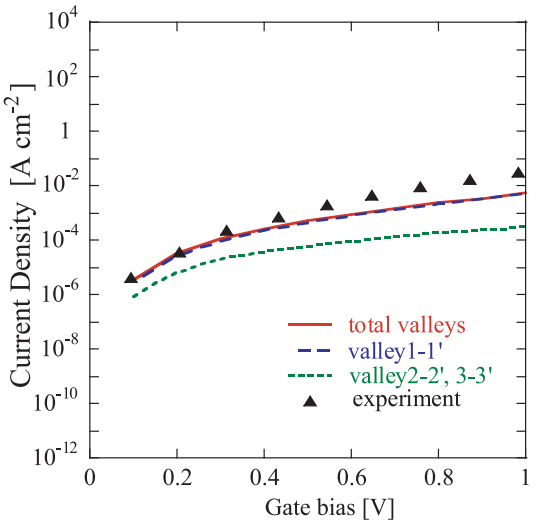

Fig. 7. The gate current density from the QBSs vs gate bias characteristics compared to the experimental data [4].

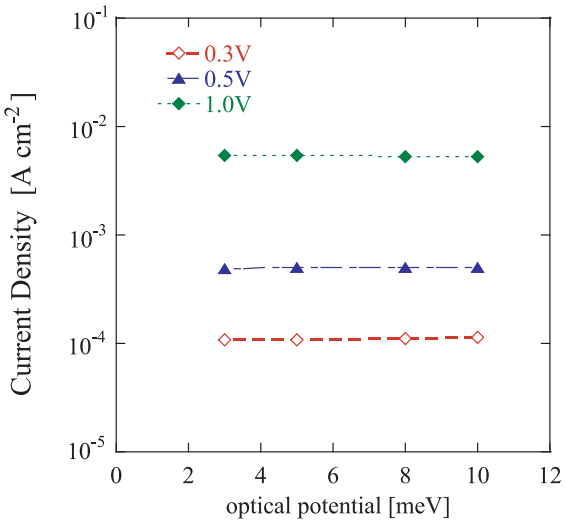

Fig. 8. The gate current density from QBSs vs the value of OP for different gate bias

transmission probability relate to the electron energy and the width of quantum-confinement. Since the effective mass along the confinement direction in valley 1-1′ is heavier than that in valley 2-2′ and 3-3′, the QBS energy levels in valley 1-1′ are lower than that in valley 2-2′ and 3-3′. So the peak energys of transmission coefficient in valley 1-1′ are lower than those in valley 2-2′ and 3-3′.

In Fig. 6, we can find that most of the current densities are comprised of those at the lowest QBS energy levels in valley 1-1′. A comparison of our result and the experimental data [4] is shown in Fig. 7, where relatively well agreement can be seen. Excellent agreement between the simulated and the experimental data are obtained over the low gate voltage range. Although slight discrepancy of the calculated current density from the experimental data is seen at higher gate voltages, it can be explained if the voltage dependence of the effective mass in the SiO_2 are taken into account as discussed in Ref. [11]. Figure 7 also shows that most of the total current density is carried by electrons in the valley 1-1′ with heavy effective mass m_l in the propagation direction, as we have already understood in the discussion of the current density spectra in Fig. 6.

Figure. 8 shows the gate current density from QBS vs the value of optical potential for different gate bias. It should be noted that introduction of the OP does not lead to any detrimental effects in the leakage current calculation as obviously shown in this figure. More importantly, the introduction has broadened the linewidth of the QBSs, which has enabled us to calculate transmission coefficient easily without assuming any empirical lifetimes.

IV. Conclusion

We have presented the results of the direct tunneling current from QBSs in MOS structure calculated on the one-dimensional NEGF formalism using the optical potential. In the simulation, both the one-dimensional quantum transport equation and the Poisson's equation are analyzed simultaneously taking into account the realistic band structures of Si. We have added optical potential, $-i\eta$, to the on-site energies only in the substrate electrode. The optical potential induces energy broadening in the triangle potential to calculate the local density of states properly. Self-consistent numerical results for n-MOSFET structures are compared with experimental data. Energy spectrum of the current density in each valley (Fig. 6) and I_G-V_G characteristics (Fig. 7) show that most of the total current density is comprised of the carrier in the valley1-1′, which have the heavy effective mass in the transport direction. Excellent agreement between the simulated and the experiment data are obtained over the low gate voltage range. Although slight discrepancy is seen at higher gate voltages, this is because it is reported that the electron effective mass in the SiO_2 decreases with increasing oxide voltage. And introduction of the optical potential does not lead to any detrimental effects in the leakage current calculation. The introduction has broadened the linewidth of the QBSs, which has enabled us to calculate transmission coefficient easily without assuming any empirical lifetimes.

References

[1] M. Karner *et*. al., Proc. of SISPAD 2006 (Monterey, USA 2006), 314.
[2] International Technology Roadmap for Semiconductors: http://www.itrs.net/
[3] D. S. Fisher *et*. al., Phys. Rev. B **23**, 6851 (1981).
[4] K. Alam *et*. al., J. Appl. Phys, **92**, 937 (2002).
[5] Khairurrijal *et*. al., J. Appl. Phys, **87**, 3000 (2000).
[6] G. Klimeck *et*. al., Appl. Phys. Lett, **67** (17), 2539 (1995).
[7] N. Yang *et*. al., IEEE Trans. Electron Devices, **46**, 1464 (1999).
[8] T. Sandu *et*. al., Physical E, **22**, 815 (2004).
[9] S. Datta, Superlattices and Microstructures, **28** (4), 253 (2000).
[10] R. Lake, VLSI DESIGN, **6**, 9 (1998).
[11] M. NAOTO *et*. al., IEICE Transactions on Electronics, **J83-C**(6), 577(2000)